Composite Structures 299 (2022) 116077

Contents lists available at ScienceDirect

Composite Structures

journal homepage: www.elsevier.com/locate/compstruct

Nacre-inspired topological design tuning the impact resistant behaviors of composite plates

Qiang Zhang [a], Hao Li [a], Yuan Liu [c], Zuoqi Zhang [a,b,*], Yanan Yuan [a,b,*]

[a] Department of Engineering Mechanics, School of Civil Engineering, Wuhan University, Wuhan 430072, PR China
[b] Engineering Research Center on Building Examination and Reinforcement Technology (Ministry of Education), Wuhan University, Wuhan 430071, PR China
[c] General Design Institute of Hubei Aerospace Technology Academy, Wuhan 430040, PR China

ARTICLE INFO

Keywords:
Staggered microstructure
Dovetail
Inverse-dovetail
Impact and penetration
Energy absorption

ABSTRACT

Nacre is well known for its high strength and toughness owing to its ingenious "brick-and-mortar" microstructure. However, its impact resistance has not been studied as well as its static properties, even though protecting fragile organs from external dynamic loadings is one of its most important functions. The current work systematically studied the impact resistant behaviors and energy absorption mechanisms of nacre-inspired composite plates with the "brick-and-mortar" organization of three typical "brick" reinforcements seen in nacre, namely, flat, dovetail and inverse-dovetail. Through the finite element method simulations, the impact stiffness, energy absorption capacity and primary working mechanisms of the composite plates during impact were analyzed. The results show that the inverse-dovetail microstructure is superior in impact stiffness in the projectile rebounding situation, while the dovetail microstructure is better for its relatively higher energy absorption capacity in both the rebounding and perforation scenarios. In the rebounding scenario the primary energy consuming mechanism is plastic deformation, whereas it converts to spalling and fragmentation in the perforation situation. The tablet aspect ratio plays a significant role in tuning the composites' impact resistant performance and working mechanisms. These findings and conclusions provide meaningful insights into the design of bioinspired composites with high impact resistance.

1. Introduction

Composites and structures with high capacity to resist impact are always highly desired in many fields such as military, aerospace, ship, and vehicle industries. Subjected to blast wave and impact loadings, these composites and structures are expected to efficiently attenuate stress wave and block projectiles by absorbing and dissipating large amounts of energy so that the damage to people and objects behind them can be minimized or avoided [1]. Load-bearing biological materials including skull, shell and some animal scales have been evolved out through billions of years of natural selection and exhibit excellent protecting function against dynamic loadings from predators and daily activities [2–6]. Therefore, learning from the structural design and impact-resistance working mechanisms of the load-bearing biological materials is definitely helpful for us to develop synthetic materials and structures with high impact-resistance performances.

Among the load-bearing biological materials, nacre has certainly received lots of attention, since it is one of the most famous load-bearing biological materials for achieving extraordinary strength and toughness from brittle mineral platelets and soft polymer matrix through relatively simple "brick-and-mortar" microstructural organization [7–9]. In natural environment, nacre plays an important role in keeping the shell from catastrophic failure by dissipating large amount of fracture energy under attacks of predators [10,11]. Although the content of aragonite crystals in the nacre is as high as 95%, the fracture toughness of nacre is more than 3000 times that of monolithic calcium carbonate [12–15], which is mainly attributed to its ingenious microstructural organization of aragonite platelets within biopolymer matrix. At the nanoscale of bone, it is found that the staggered arrangement, protein viscosity and mineral fraction work cooperatively to promote the stress wave attenuations [16]. Many decent experimental studies have revealed that the interface between aragonite platelets is not flat but with finer sub-microstructure features such as surface asperity, mineral bridge and waviness [15,17–28]. These sub-microscale structures have been demonstrated playing important roles in the strengthening and toughening mechanism of nacre [7,29–33]. As shown in Fig. 1a, the iridescent layer of an

* Corresponding authors at: Department of Engineering Mechanics, School of Civil Engineering, Wuhan University, Wuhan 430072, PR China.
E-mail addresses: zhang_zuoqi@whu.edu.cn (Z. Zhang), yuanyn@whu.edu.cn (Y. Yuan).

https://doi.org/10.1016/j.compstruct.2022.116077
Received 20 January 2022; Received in revised form 12 May 2022; Accepted 4 August 2022
Available online 8 August 2022

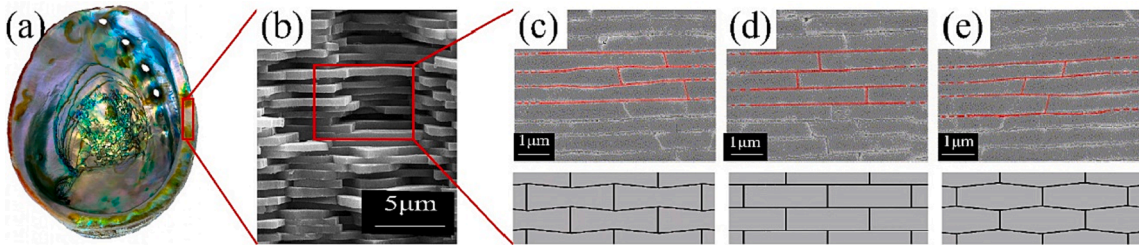

Fig. 1. (a) Nacreous layer of an abalone shell, (b) scanning electron micrograph (SEM) of a facture surface of nacre, and three types of platelet reinforcement illustrated as (c) dovetail, (d) flat and (e) inverse-dovetail platelet, respectively [34].

abalone shell is nacre, also named as mother of pearl, since pearls are cultured there. Fig. 1b presents the scanning electron micrograph of a facture surface of nacre, and the stacked mineral "bricks" can be seen clearly. Enlarged views of these "brick-and-mortar" microstructures show that the platelet reinforcements can be generally classified into three types according to their geometrical characteristics, see Fig. 1c-e [34], herein termed as dovetail (c), flat (d) and inverse-dovetail platelet (e), respectively. The dovetail platelets have thicker and larger ends analogous to the shape of dovetails, the flat platelets have uniform thickness, whereas the inverse-dovetail platelets have thinner and smaller ends contrary to the dovetail ones. The dovetail structure is well known for its interlocking effect when the neighboring reinforcements slide against each other [20,35]. The interlocking effect can make a great contribution in stiffening, strengthening and toughening the composites [27,28,34–43]. However, it is still not well understood why the three typical structures coexist in load-bearing biological materials, especially with the dynamic loading conditions taken into consideration.

A number of nacre-inspired composites have been fabricated in laboratories [1,44]. For instance, Tang et al. using sequential deposition method manufactured nanostructured artificial nacre achieving well-ordered brick-and-mortar arrangement of polyelectrolytes and clays [45] Munch et al. emulated nacre's toughening mechanisms and synthesized tough nacre-like composites with aluminum oxide and polymethyl methacrylate by freeze-casting method [46] Most recently, Yin et al. proposed a nacre-like laminated glass that duplicates the 3D "brick-and-mortar" arrangement and exhibits significantly improved toughness and impact resistance [47]. Nonetheless, the interlocking submicrostructural features had not got sufficient attention in these nacre-inspired material design and fabrication. Through FEM simulations, Flores-Johnson et al. [1] investigated the ballistic performance of a nacre-inspired aluminum composite plate featuring tablet waviness and cohesive interface. Their results showed that the nacre-inspired plate can provide a better ballistic performance than their bulk and continuous layer counterparts, but the performance improvement is dependent on the plate thickness and projectile velocity. Tran et al. [44] performed FEM studies on the nacre-inspired composite plates subjected to underwater impulsive loadings and found that inter-laminar debonding was reduced in the bioinspired structures due to the interlocking mechanism associated with the dog-bone shape design of tablets. In these existing studies, the key question is still yet to be answered: what effects do the dovetail and inverse-dovetail platelet reinforcements have, especially with comparison to the flat ones. Our current paper was aimed to systematically study the impact resistant performance of nacre-inspired composites with different topological design of reinforcement tablets, namely, dovetail, inverse-dovetail and flat.

In this paper, aluminum alloy/epoxy composite plates with the aforementioned three kinds of nacre-inspired microstructures were modeled with Abaqus/Explicit, and a hemispherical projectile was used to impact the plates at a wide range of velocity. Through a series of FEM simulations, the impact resistant behaviors and properties were compared among the composite plates. Several geometrical parameters such as the aspect ratio and inclination angle of reinforcement platelet were also studied to provide useful guidance for practical design. The dominant mechanism of impact energy absorption in different scenarios were analyzed. The remaining of the paper is organized as follows. Section 2 depicts the simulation setup, Section 3 gives the numerical results and discussions. Finally, Section 4 summarizes the main conclusions.

2. Simulation setup

2.1. Geometrical model

The geometrical model for a typical dovetail tablet of aluminum alloy was shown in Fig. 2a. The length and width of tablet (square) are the same and denoted by c, the height at the center point is d, the height at the edge center is b, the height at the outer corner is a. To ensure the tablets well assembled to form a composite plate, the following relation is always satisfied in all our models

$$a + d = 2b \tag{1}$$

indicating that the value of b is always between that of a and d. The aspect ratio of reinforcement tablet is defined as

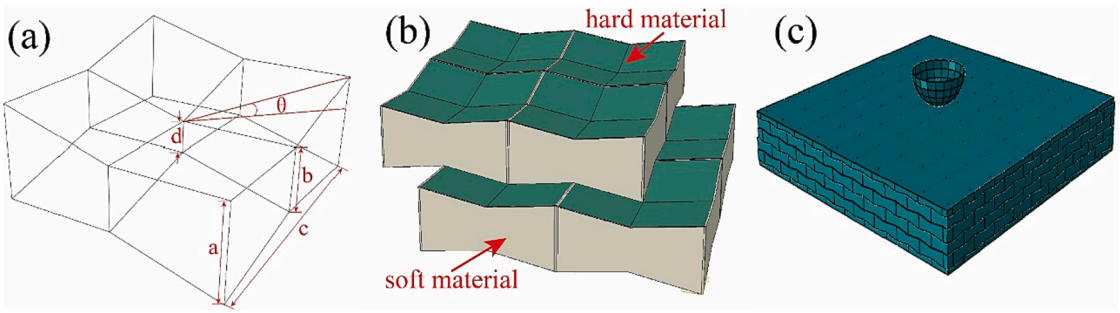

Fig. 2. Illustration of a generalized reinforcement platelet (a), the staggered organization of platelets in three-dimensional space (b), and the macroscopic model for the composite plate under ballistic impact (c).

$$\lambda = \frac{2c}{a+d} = \frac{c}{b} \tag{2}$$

The angle between the inclined surface and the horizontal plane is defined as the inclination angle θ, which is related to the dimensions a, c and d by the following equation

$$\tan\theta = \frac{a-d}{\sqrt{2}c} \tag{3}$$

$\theta > 0$, a is larger than d, and the reinforcement tablet shape is dovetail; when$\theta = 0$, a, b and d are all the same, and the flat shape was obtained; when$\theta < 0$, a is less than d, and the inverse-dovetail shape is acquired. Eqs. (1)-(3) tells that the tablet geometry can be also completely determined by the parameters a, c, λ and θ.

As shown in Fig. 2b, the hard tablets (dark green color in the online version) are merged together with soft adhesives (grey color in the online version) in a staggered pattern in three-dimensional space. One can see that each layer is displaced with respect to its upper or/and lower adjacent layers in such a way that every pair of upper-lower neighboring tablets are 1/4 overlapped with each other.

2.2. Finite element modelling

Fig. 2c shows the macroscopic composite plate, which can be seen as a repeated assembly of Fig. 2b. The composite plate contains five layers of tablets, with each layer having a thickness of 10 mm and 20*20 reinforcement tablets. A rigid hemisphere with a certain initial velocity was shot to collide with the nacre-inspired composite plate. The radius of the hemisphere projectile is set to be comparable to the tablet width, i.e., $r = c$. The mass of the projectile is assumed 5 g. The hard tablets were meshed with an 8-node linear brick element C3D8, while the soft interfaces inside each layer were meshed with 8-node three-dimensional cohesive element COH3D8. All the seed size was chosen to be $0.17c \times 0.17c \times 0.17c$, and well passed the test of mesh convergence. Cohesive contact property was defined between the adjacent layers to simulate the mechanical behaviors of soft interfaces between them. The rigid-body movement of the composite plate was first constrained, and then the four vertical surface planes were all fixed. The projectile was just placed on the top surface of the composite plate and given an initial velocity (5–500 m/s) perpendicular to the plate, while the other degrees of freedom were fixed. The automatic time incrementation scheme in Abaqus/Explicit was adopted, which can ensure that a stable time increment is employed. Mesh sensitivity analysis has been conducted, confirming that the current level of refinement was enough to obtain a converged solution. It is also worth noting that the plate size has been verified large enough to get converged results for our simulations. Specifically, the simulation results on larger plates containing 5*30*30 and 5*40*40 tablets have been shown almost the same as those obtained from the 5*20*20 composite plate, with a deviation of less than 3%.

2.3. Material models

As a typical example, the hard tablet material was taken as an aluminum alloy, while the soft matrix material was chosen to be an epoxy resin. Johnson-Cook (JC) material model was utilized for the aluminum alloy, as it has been successfully applied to the ballistic impact simulations of aluminum alloy plates [1]. For the epoxy resin interface, a traction-separation cohesive law was defined. For the sake of completeness, a brief explanation of each material model is provided below.

The JC constitutive model is an empirical model for studying the dynamics of metal materials under impact loads. In JC model, the equivalent stress σ_{eq} is given in the following form

$$\sigma_{eq} = \left(A + B\varepsilon_{eq}^{n}\right)\left(1 + C\ln\dot{\varepsilon}_{eq}^{*}\right)\left(1 - T^{*m}\right) \tag{4}$$

Table 1
Material parameters in finite element modeling [16].

Aluminum alloy (hard)	
Density ρ (kg/m^3)	2700
Elastic modulus: E (GPa)	70
Poisson's ratio:ν	0.3
Inelastic heat fraction	0.9
Specific heat (J/kg K)	910
Hardening coefficient A (MPa)	520
Hardening coefficient B (MPa)	477
Hardening coefficient n	0.52
Epsilon dot zero $\dot{\varepsilon}_0$ (s^{-1})	0.0005
C	0.001
Transition Temperature (K)	293
Melting Temperature (K)	893
m	1
D1, D2, D3, D4, D5, and u^f	0.049, −3.465, 0.016, 1.099,0.009, and 0.096

where the coefficients A, B, C, and the power m and n are material constants, ε_{eq} denotes the equivalent plastic strain, $\dot{\varepsilon}_{eq}^{*}$ is the dimensionless plastic strain rate defined as the ratio of the equivalent plastic strain rate to a user-defined strain rate$\dot{\varepsilon}_{eq}/\dot{\varepsilon}_0$, the homologous temperature T^* is defined as$T^* = (T - T_r)/(T_m - T_r)$, with$T$, T_r and T_m referring to the absolute temperature, the room temperature and the melting temperature, respectively.

In the process of transient plastic deformation, the material may soften due to rapid local heating. ABAQUS/Explicit allows to research on softening of materials by computing the increase in the heat flux per unit volume,

$$r_{pl} = \eta\sigma : \dot{\varepsilon}_{pl} \tag{5}$$

In the above equation, η is the inelastic heat fraction, σ is the stress and $\dot{\varepsilon}_{pl}$ is the plastic strain rate. It can also be expressed as

$$r_{pl} = \rho C_p \Delta T \tag{6}$$

Here ρ is the material density, C_p is the specific heat and ΔT is the temperature variation. Combining Eqs. (2) and (3), the temperature rise can be obtained by integration

$$\Delta T = \int_0^{\varepsilon_{pl}} \frac{\eta\sigma d\varepsilon_{pl}}{\rho C_p} \tag{7}$$

The JC fracture criterion is based on damage accumulation at every element integration point. The accumulative damage parameter is defined as below

$$D_{JC} = \sum \frac{\Delta\varepsilon_{eq}}{\varepsilon_f^{JC}} \tag{8}$$

where $\Delta\varepsilon_{eq}$ is the increment equivalent plastic strain, and

$$\varepsilon_f^{JC} = (D_1 + D_2\exp(D_3\sigma^*))(1 + D_4\ln\dot{\varepsilon}_{eq}^{*})(1 + D_5T^*) \tag{9}$$

is the equivalent fracture strain, and $D_i (i = 1...5)$ are material constants; $\sigma^* = \sigma_m/\sigma_{eq}$ is the stress triaxiality, with σ_m as the hydrostatic stress. When $D_{JC} = 1$, the damage initiates and the material starts to degrade. Once the damage starts, the effective plastic displacement u_{eq} is calculated by

$$u_{eq} = L\varepsilon_{eq} \tag{10}$$

in which L is the characteristic length of element. Assuming a linear relationship between the damage variable d and the effective plastic displacementu_{eq}, the damage variable is determined by

$$d = u_{eq}/u_{eq}^{f}$$

Here u_{eq}^{f} is the effective plastic displacement when the material is completely failure. Once complete failure occurs ($d = 1$), the failed elements will be removed from the model mesh. All the typical material

Table 2
Material parameters for the interface cohesive element.

Epoxy material (soft)	
Density ρ (kg/m^3)	1350
Elastic modulus: E (GPa)	3.1
Shear modulus G_1, G_2 (Gpa)	1.55
Nominal stress σ_n^0(MPa)	85.5
Shear stress σ_s^0 and σ_t^0 (MPa)	70
G_{IC} (J/m^2)	1680
G_{IIC} (J/m^2)	3570
K_n (N/mm)	1373.3
K_s (N/mm)	493.3
K_t (N/mm)	493.3

parameters for the aluminum alloy were listed in Table 1.

The epoxy resin matrix is modeled as a cohesive interface whose constitutive mechanical behaviors are governed by the following traction-separation law

$$\sigma_i = K_i\delta_i i = n, s, t \tag{12}$$

Here σ_i and δ_i denote the traction stress vector and separation, respectively. n represents the normal while s and t are shear directions. The maximum stress criterion was applied to define damage initiation

$$\max\left\{\frac{\sigma_n}{\sigma_n^0}, \frac{\sigma_s}{\sigma_s^0}, \frac{\sigma_t}{\sigma_t^0}\right\} = 1 \tag{13}$$

in whichσ_n^0, σ_s^0 and σ_t^0 are the critical stresses of damage initiation in the respective directions.

Once the corresponding damage initiation criterion has been reached, the rate of degradation of the material stiffness is described by a damage variable D which ranges from zero to one as the interface damage initiates and develops to complete failure. The failure criterion for predicting delamination propagation under mixed-mode loading is expressed by the energy release rates associated with Modes I, II and III [48]. For a linear softening process, the damage variable D for delamination evolution is defined as

$$D = \frac{\delta_m^f\left(\delta_m^{\max} - \delta_m^0\right)}{\delta_m^{\max}\left(\delta_m^f - \delta_m^0\right)},\ D \in [0, 1] \tag{14}$$

where the mixed-mode displacement (normal, sliding and tearing) δ_m is given by

$$\delta_m = \sqrt{\delta_n^2 + \delta_s^2 + \delta_t^2} \tag{15}$$

$\delta_m^{\max}$ refers to the maximum mixed-mode displacement attained during the loading history, δ_m^f is the mixed-mode displacement at complete failure, and δ_m^0 is the effective displacement at damage initiation. δ_m^f can be defined according to the Benzeggagh-Kenane (BK) fracture energy based criterion [49]

$$\delta_m^f = \begin{cases} \frac{2}{K\delta_m^0}\left[G_{IC} + (G_{IIC} - G_{IC})\left(\frac{\beta^2}{1+\beta^2}\right)^{\eta}\right] & \delta_n > 0 \\ \sqrt{\left(\delta_s^f\right)^2 + \left(\delta_t^f\right)^2} & \delta_n \leqslant 0 \end{cases} \tag{16}$$

In the above equation, η is the BK power law parameter that can be determined using a least-square fit from a set of mixed-mode bending experiments; $\beta = \frac{\delta_s}{\delta_n}$ is the mode mixity ratio; $\beta = 0$ indicates that the mode I fracture is dominant, while $\beta = \infty$ or $\eta = 0$ suggest that the mode II fracture is dominant. The typical parameters for the interface cohesive material were given in Table 2.

2.4. Energy balance

According to the principle of energy conservation, the total energy absorbed by the composite plate should be equal to the energy loss of the projectile

$$E_{ab} = \frac{1}{2}mV_{ini}^2 - \frac{1}{2}mV_{res}^2 \tag{17}$$

where m is the mass of the projectile, V_{init} and V_{res} are the initial and residual velocity of projectile before and after the impact, respectively. The energy absorption efficiency is defined as the ratio of the absorbed energy by composite plate over the initial dynamic energy of projectile

$$\eta = 2E_{ab}/mV_{ini}^2 \tag{18}$$

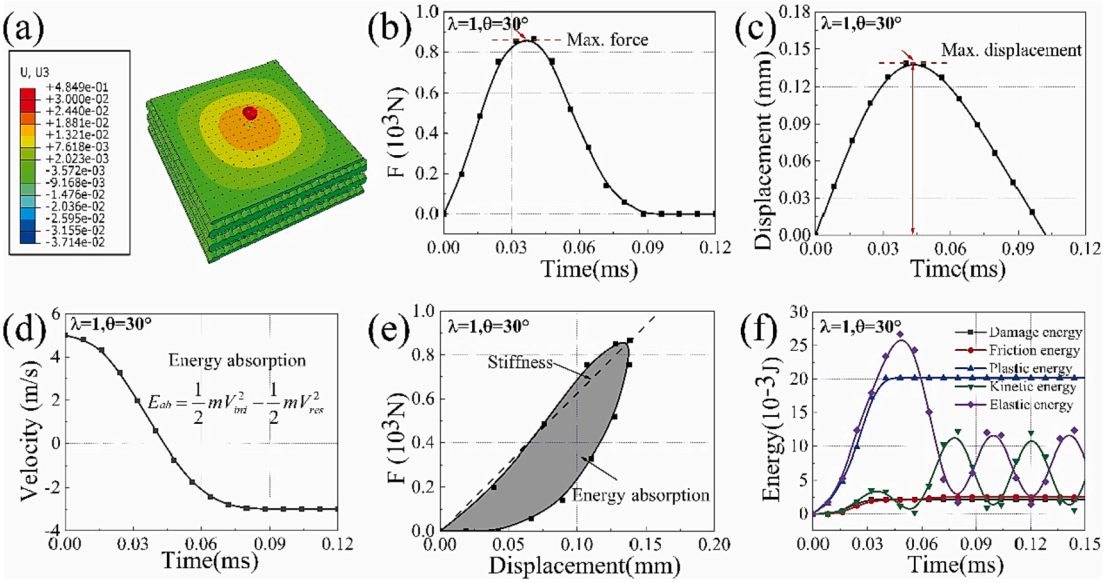

Fig. 3. Typical rebounding responses of a composite plate with $\lambda = 1$, $\theta = 30^\circ$ under $V_{ini} = 5$ m/s for example: Contour of out-of-plane displacement (a); time history of impact force (b), projectile displacement (c), and projectile velocity (d); curve of impact force versus displacement (e); different energy components varying over time (f).

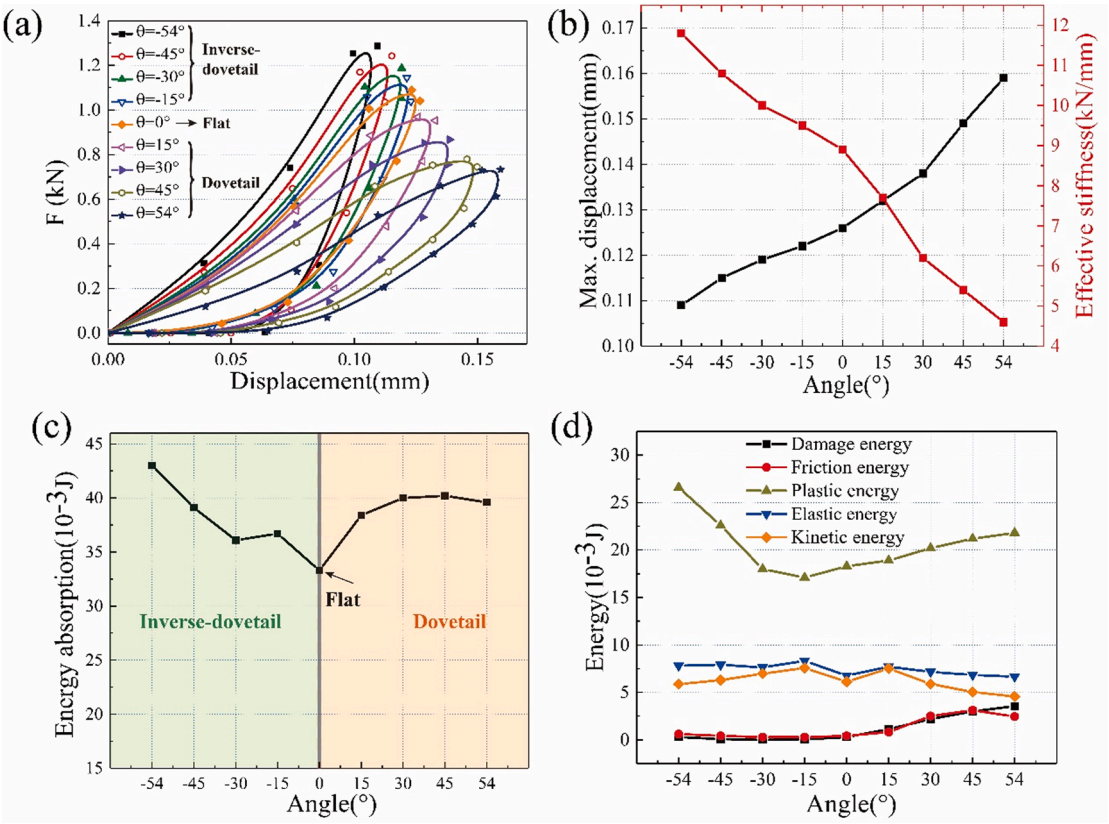

Fig. 4. Rebounding response comparison among the dovetail, flat and inverse-dovetail micro-structured composite plates (e.g., $\lambda = 1, V_{ini} = 5m/s$ here): (a) the impact force-displacement curves for different inclination angles; the variation of (b) the maximum displacement and effective stiffness, (c) the energy absorption, and (d) the primary energy components in the composite plates with respect to the inclination angle.

In particular, the energy absorbed by the composite plate primarily consists of the damage energy, friction energy, plastic energy, kinetic energy and elastic energy, either dissipated or stored in the composite plate. In our simulations, the energy balance is guaranteed by checking the dynamic energy loss of the projectile, and the dissipated and stored energy in the composite plate, and ensuring them equal to each other (the relative difference less than 1%).

3. Results and discussion

3.1. Rebounding behaviors

When the impact energy is relatively small, the projectile will be rebounded after impact. Fig. 3 shows typical rebounding responses, with an example of composite plate which has an inclination angle $\theta = 30^{\circ}$ (dovetail shape) and reinforcement aspect ratio $\lambda = 1$, subjected to an impact of initial velocity $V_{\text{ini}} = 5$ m/s. Fig. 3a presents the out-of-plane displacement contour, with the largest value at the plate center (i.e., impact point) and radically decreasing to the boundary in a circular pattern. Fig. 3b-d show the time history of impact force, displacement and velocity of the projectile, respectively. The maximum force F_{max}, displacement U_{max}, and dynamic energy loss E_{ab} of the projectile are highlighted. Note that the minus value of projectile velocity indicates that the projectile was rebounded and pushed away from the composite plate. Based on Fig. 3b and c, we can plot the force-displacement curve during the impact process, as shown in Fig. 3e. From this curve, two additional quantities can be calculated to evaluate the impact resistance of the nacre-inspired composite plate, namely the effective impact stiffness K_{b} and energy absorption capacity E_{ab}. The effective impact stiffness K_{b} is defined as the slope of the secant line connecting the origin and the peak points (see the dashed line in Fig. 3e), and the energy absorption capacity E_{ab} is defined as the shaded area bounded by the force-displacement loop. According to the principle of energy conservation, it is evident that the energy absorption capacity of the plate should be the same as the dynamic energy loss of the projectile, and thus the same notation is adopted for both of them. Fig. 3f plots the time history of primary energy components of nacre-inspired composite plate including damage energy, friction energy, plastic energy, kinetic energy, and elastic energy during the impact. The first three components are irreversibly dissipated by the composite plate through damage and failure related mechanisms, while the last two are energy stored in the composite plate. As mentioned in Section 2.4, the summation of these energy components, i.e., the total energy absorption of the plate, is equal to the energy loss of the projectile because of energy conservation. In particular, one can see in the example that around 0.045 ms the projectile velocity became zero, and correspondingly the impact interaction, out-of-plane displacement, elastic deformation energy, damage energy, friction energy and plastic energy respectively reached their maxima; around 0.1 ms the projectile flied away from the composite plate at a constant velocity, and correspondingly the composite plate was left vibrating freely, with its kinetic energy and elastic energy oscillating out of phase. All the phenomena are physically sensible.

Fig. 4 compares the impact responses of composite plates as the inclination angle varies from $-54^{\circ}$to 54°, corresponding to the micro-structures change from inverse-dovetail to dovetail type. Generally, as the inclination angle increases, the impact force-displacement loop gradually becomes low and thin (see Fig. 4a); correspondingly, the effective impact stiffness (black curve) gradually decreases, and the maximum displacement (red curve) gradually increases, as shown Fig. 4b. The stiffness decrease with the inclination angle mainly originates from the increasing inhomogeneity of the longitudinal stress in the reinforcement tablets. Specifically, the maximum axial force in the

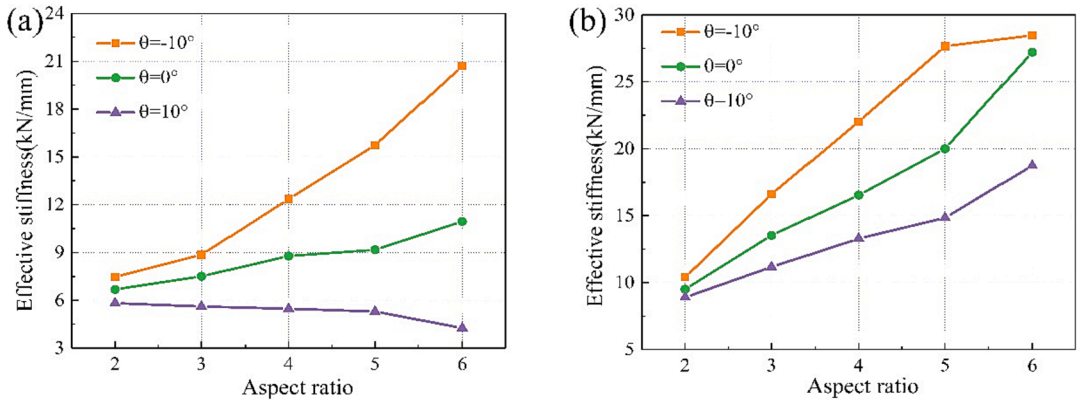

Fig. 5. The effective stiffness among the dovetail, flat and inverse-dovetail microstructures for different platelet aspect ratios. The impact initial velocity is (a) 5 m/s and (b) 20 m/s.

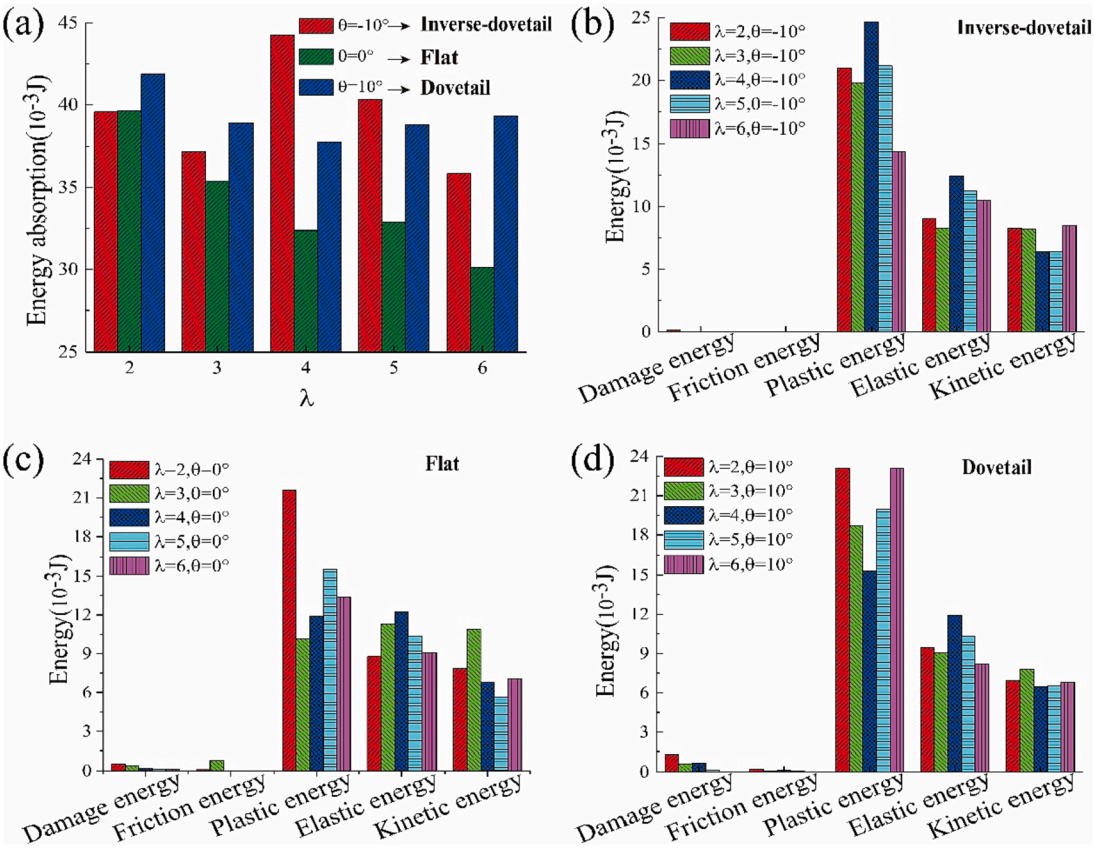

Fig. 6. Histogram of the total energy absorption (a), and different energy dissipation mechanisms for the inverse-dovetail ($\theta = -10°$, b), flat ($\theta = 0°$, c) and dovetail ($\theta = 10°$, d) microstructures with a variety of aspect ratio λ considered. All the initial impact velocity is 5 m/s.

tablets usually presents at their central cross-section according to the shear-lag theory; on the other hand, as the inclination angle increases (from inverse-dovetail to dovetail), the tablets have smaller and smaller central cross-sections; as a result, there is larger and larger axial stress around the central regions, and the total extension of the tablets becomes larger and larger under the same external loadings; finally, the composites show smaller and smaller stiffness. Fig. 4c suggests a non-monotonic variation of the energy absorption over the increase of the inclination angle, and the flat microstructure gives the smallest energy absorption. Comparing the energy components in Fig. 4d, one can see that the energy absorbed by the composite plates is mainly converted into their plastic and elastic deformation energy, and kinetic energy. The inverse-dovetail and dovetail microstructures exhibit significantly higher plastic energy dissipation than the flat microstructure, because the wavy interfaces and non-uniform tablets suffer higher stress concentration and more plastic deformation. In addition, the damage and friction energy are slightly larger for the dovetail microstructured composite plates, since the interlocking effect increases the interface stress and tends to generate more interface debonding and inter-tablet sliding.

The influences of aspect ratio λ on the impact responses of nacre-inspired composite plates were also investigated. Fig. 5a shows the effective stiffness of the projectile with variable aspect ratio for the three typical microstructures: dovetail ($\theta = 10^{\circ}$), flat ($\theta = 0^{\circ}$), and inverse-dovetail ($\theta = -10^{\circ}$) under the initial impact velocity 5 m/s. As the aspect ratio increases, the effective impact stiffness slightly decreases for

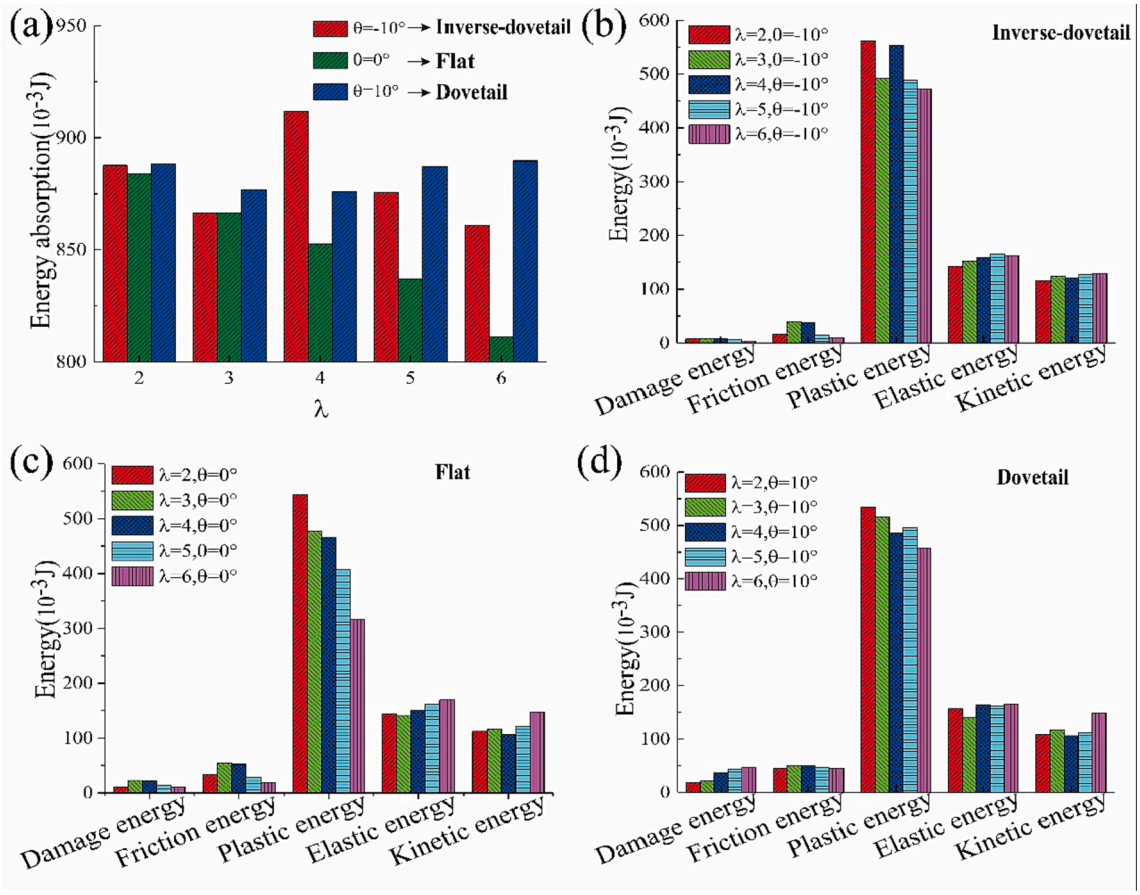

Fig. 7. Histogram of the total energy absorption (a), and different energy dissipation mechanisms for the inverse-dovetail ($\theta = -10°$, b), flat ($\theta = 0°$, c) and dovetail ($\theta = 10°$, d) microstructures with a variety of aspect ratio λ considered. All the initial impact velocity is 20 m/s.

the dovetail microstructure while significantly increases for the flat and inverse-dovetail microstructures. When the aspect ratio is relatively small, the composite plate deformation is dominated by the inter-tablet dislocation and slippage. When the aspect ratio becomes larger and larger, the deformation gradually becomes dominated by the extension of tablets and the bending of the whole plate. For the dovetail microstructure with a smaller middle cross-section, the stress concentration around the middle cross-section increases and consequently the tablet extension increases with the increasing aspect ratio. This mainly accounts for its effective impact stiffness decrease with the tablet aspect ratio. In contrary, the flat and inverse-dovetail microstructures have no such stress concentration issue so that their effective impact stiffness increases with the tablet aspect ratio, so does their effective static stiffness. Fig. 5b shows their effective stiffness under a higher initial impact velocity 20 m/s, and we can see the effective impact stiffness of then dovetail microstructured composites also change to be increase with the aspect ratio. This is because the mechanical interlocking effect starts to contribute as the inter-tablet deformation becomes larger under

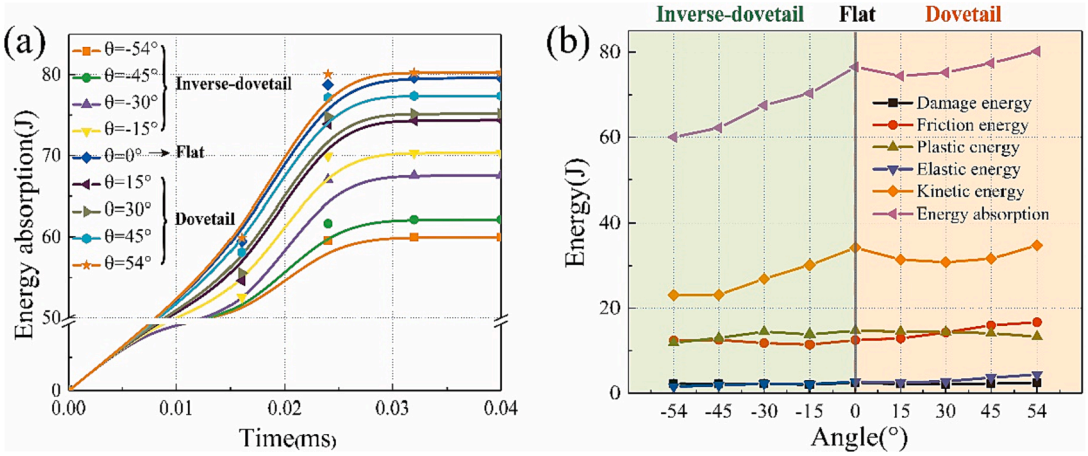

Fig. 8. Perforation response comparison among the dovetail, flat and inverse-dovetail micro-structured composite plates ($\lambda = 1, V_{ini} = 500m/s$ here): (a) the history of energy absorption, (b) the damage energy, friction energy, plastic energy, kinetic energy and total energy absorption in the composite plates varying with the inclination angle.

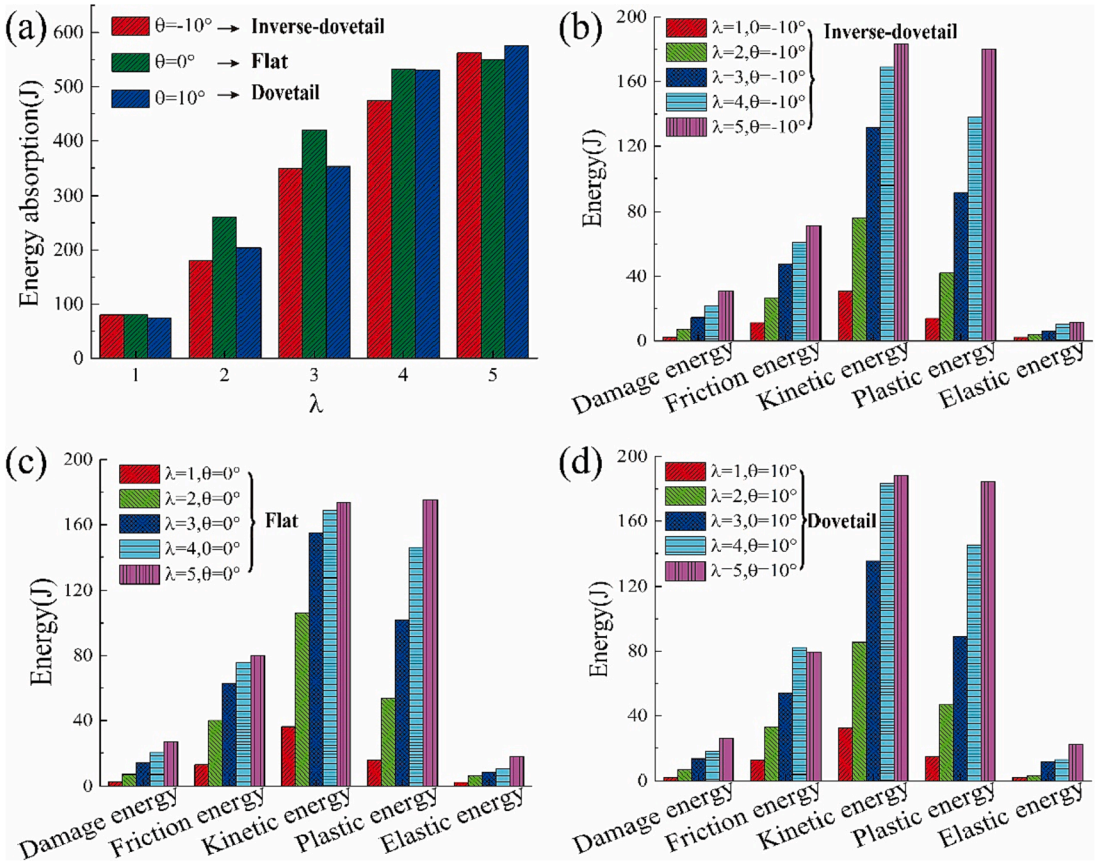

Fig. 9. Histogram of dissipation energy by different mechanisms for the inverse-dovetail ($\theta = -10°$) (a), flat ($\theta = 0°$) (b) and dovetail ($\theta = 10°$) microstructures (c), and **their total energy absorption (d), with a** variety of aspect ratios λ considered. All the initial impact velocity is 500 m/s.

the higher impact velocity. This point can be further confirmed by the increase of friction energy dissipation with the initial impact velocity increasing from 5 m/s (see Fig. 6) to 20 m/s (see Fig. 7).

Fig. 6 and Fig. 7 show the total energy absorption and different energy components of the nacre-inspired composite plates with different tablet aspect ratios, under the initial projectile velocity 5 m/s and 20 m/s, respectively. Generally speaking, in the impact rebounding scenario, with the tablet aspect ratio increasing the total energy absorption always decreases for the flat microstructure, but it first increases and then decreases for the inverse-dovetail microstructure while first decreases and then increases for the dovetail microstructure. Among the energy components, the largest one is the plastic energy and followed by the elastic and kinetic energy. When the initial velocity of the projectile is small, the impact force and related stress are also small so that material damage hardly happens, and thus the damage and friction energy components are trivial as shown in Fig. 6b-d. In contrast, the contribution of material damage and inter-tablet friction becomes visible when the initial impact velocity becomes large, see Fig. 7b-d. As a result, with the increasing aspect ratio of reinforcement tablets, the varying trends of total energy absorption are the same as those of the plastic energy at the low impact velocity, whereas the varying trends of the total energy deviate from those of the plastic energy at the high impact velocity.

3.2. Perforation behaviors

As the initial velocity of projectile increases beyond the ballistic limit (70–400 m/s depending on microstructures), the impact behavior goes into the perforating scenario from rebounding. In the perforation cases, the projectile penetrates and goes through the composite plates, and the effective impact stiffness becomes not so important. Fig. 8 compares the history of energy absorption and different energy components among the nacre-inspired composite plates with variable microstructures, the initial projectile velocity 500 m/s taken here as an example. Fig. 8a shows that the total energy absorption, i.e., the kinetic energy loss of the projectile, increases with time as the projectile penetrates the composite plates, and finally becomes a constant after the projectile perforates the plates. As the inclination angle varies from -54° to54°, the total energy absorption by the nacre-inspired composite plates generally increases, suggesting that the dovetail microstructures yields better resistance to the impact perforation. Fig. 8b plots the total energy and major components within the composite plates varying with respect to the inclination angle. One can see that the kinetic energy of composite plates accounts for more than 35% of the total energy consumption, and is the primary mechanism of energy absorption. It is worth noting that the kinetic energy with composite plates include the vibration kinetic energy of the remaining composite plates and the flying kinetic energy of the fragments produced during the perforation. The secondary energy consumption mechanisms are plastic and friction energy dissipation by the irreversible deformation and relative sliding of reinforcement tablets, and each of them makes up more than 20% of the total energy absorption. Due to the mechanical interlocking effect, the friction mechanism contributes a little more with the dovetail microstructures than that with the inverse-dovetail microstructures. Elastic deformation and material damage consume a trivial part of energy, probably because the elastic deformation and damage are highly localized due to the high impact velocity.

To investigate the influences of aspect ratio λ on the impact responses in perforation cases, the three microstructures ($\theta = -10^{\circ}, 0^{\circ}, 10^{\circ}$) with a variety of aspect ratios λ were considered in Fig. 9, with an initial impact velocity 500 m/s. As the aspect ratio increases from 1 to 5, the total energy absorption increases for all the three topology designs, though the increasing amount gradually becomes small, see Fig. 9a. For

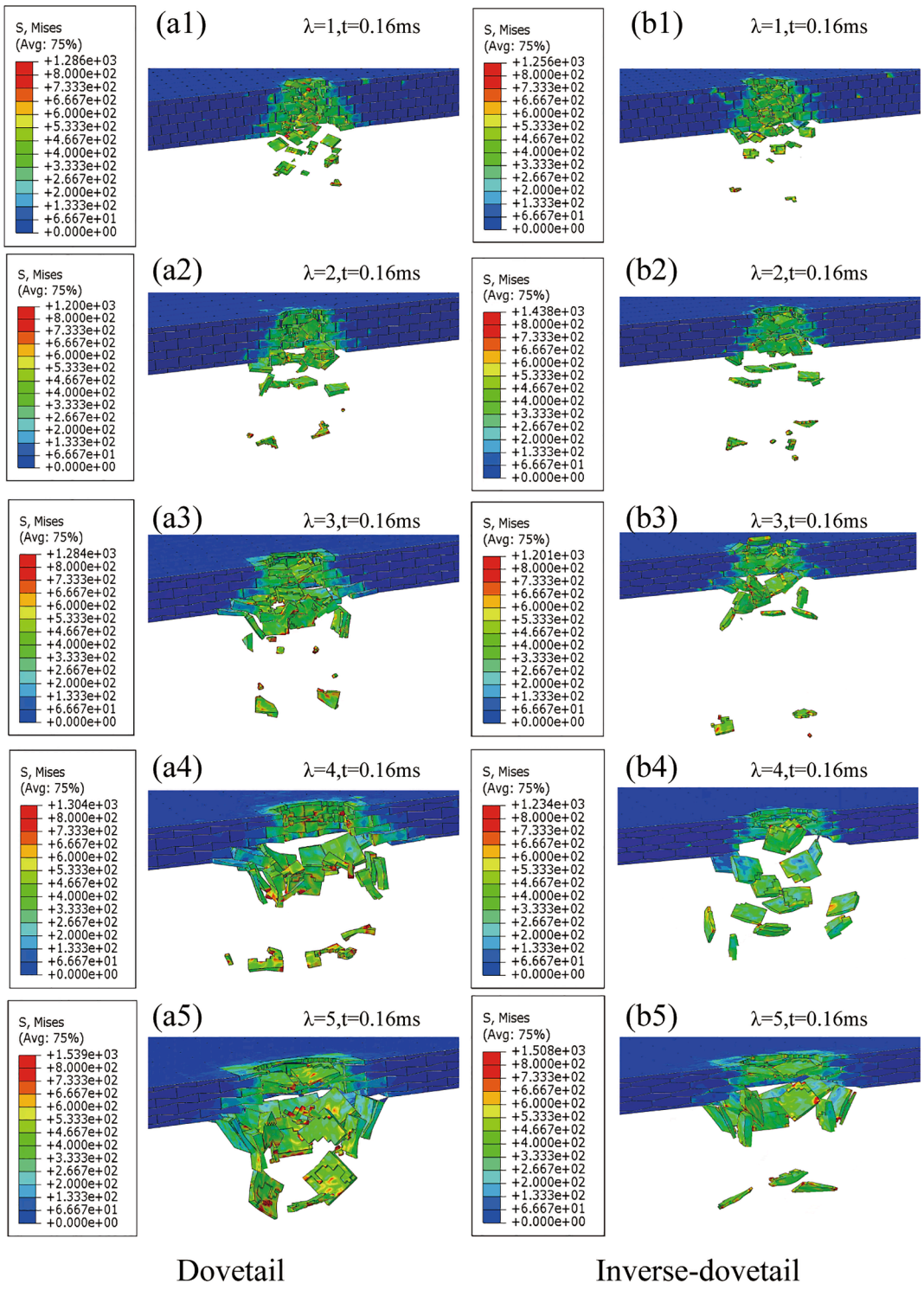

Fig. 10. Mises stress contour of nacre-like composite plates at the moment t = 0.16 *ms* under $V_{ini} = 500m/s$ for dovetail microstructures (a1-a5) and inverse-dovetail microstructures (b1-b5), with platelet aspect ratioλ = 1, 2, 3, 4 and 5.

the small aspect ratios (e.g., 1–3), the flat microstructure outperforms the inverse-dovetail and dovetail microstructures in term of the energy absorption. As the aspect ratio increases, the dovetail microstructure gradually surpasses the other two. The energy components varying with the aspect ratio for the three microstructured composites were shown in Fig. 9b-c. One can see that the plastic and kinetic energy are always the first two primary components regardless of the topological design and tablet aspect ratio. In particular, when the aspect ratio is relatively small, the kinetic energy is the largest component because of the spalling effect. When the aspect ratio is large (e.g., 5), the component of plastic energy becomes comparable to the kinetic component, that should be attributed to the higher bending stiffness and stress level induced by the larger tablets. This can be confirmed by Fig. 10, from which one can see that the Mises stress increases and more materials go into plastic deformation as the aspect ratio increases.

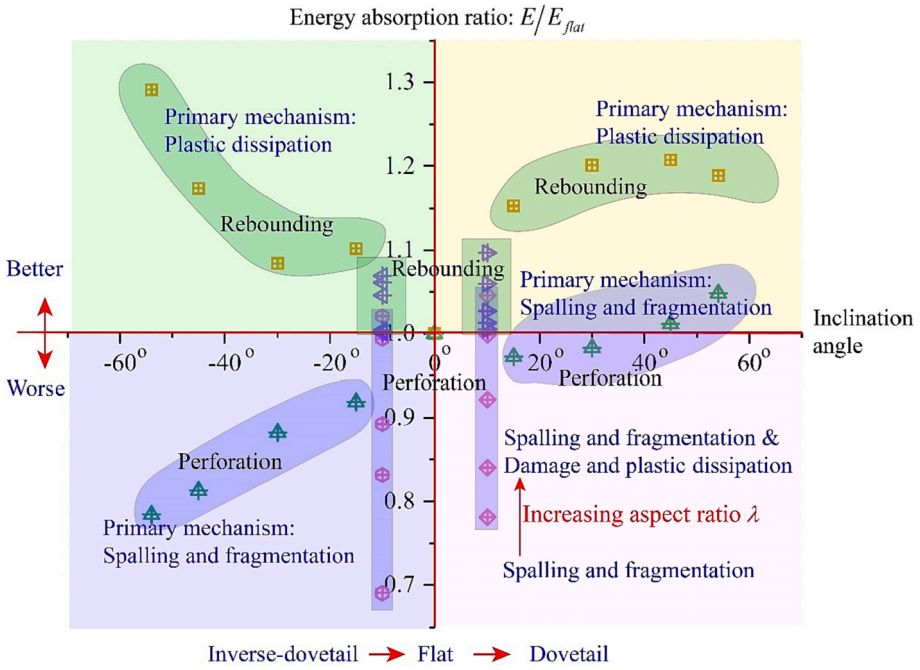

Fig. 11. Phase diagram of impacting resisting mechanism with different microstructure designs.

3.3. Summary of the energy absorption and dominant mechanisms

Fig. 11 summaries the relative energy absorption of the three microstructured composite plates and their major working mechanisms. The ordinate E/E_{flat} represents the relative energy absorption normalized by the energy absorption of flat microstructured plates. In the rebounding scenario, the dovetail and inverse-dovetail microstructures usually absorb more impact energy, and the primary dominant working mechanism is plastic dissipation followed by the elastic energy and the kinetic energy. The damage and friction energy are trivial when the impact velocity is low. In the perforation scenario, the energy absorption capacity generally increases with the inclination angle, indicating that the dovetail microstructure performs best among the three kinds of microstructures. The primary energy component is the kinetic energy due to the fragmentation and spalling effects, but the plastic dissipation gradually increases and becomes comparable to and even surpassing the kinetic component as the aspect ratio increases. In addition, the damage and friction mechanisms also contribute significantly in the perforation situation.

4. Conclusions

The current paper established three types of nacre-inspired composite plates, namely dovetail, flat, and inverse-dovetail microstructured composite plates, and through FEM simulations studied their impact resistance capacity under both low and high impact velocities. The following major conclusions can be drawn:

(1) In the rebounding cases, the inverse-dovetail and flat microstructures show higher impact stiffness than the dovetail, but the dovetail and inverse-dovetail exhibit larger energy absorption capacity than the flat. With the tablet aspect ratio increasing, the impact stiffness generally increases regardless of the microstructure, while the varying of energy absorption depends on the microstructure. The major part of energy absorbed by the composite plates is converted into their plastic and elastic deformation energy. The damage and inter-tablet friction also play a distinct role in the energy absorption as the impact velocity becomes relatively high.

(2) In the perforation scenario, the dovetail microstructures with relatively large inclination angles outperform the inverse-dovetail and flat microstructures in the energy absorption capacity, suggesting their good impact resistance. Owing to the effect of spalling and fragmentation, the kinetic energy constitutes the primary part of total energy absorption. With the increase of tablet aspect ratio, the energy absorption increases for all the three types of microstructures, and its difference resulted from microstructures becomes insignificant.

(3) Considering the working conditions of rebounding and perforation, the three types of nacre-inspired composite plates demonstrate different impact resistant performance and working mechanisms. From perspective of material selection and design, the inverse-dovetail microstructure is recommended for its relatively higher impact stiffness (correspondingly, smaller deflection) in the rebounding situation, while the dovetail microstructure is preferred for its relatively higher energy absorption capacity. Noteworthy, the advantage of flat microstructure is also evident because of its simplicity and cost efficiency in terms of design and fabrication processes.

The findings and conclusions above provide meaningful insights into the design of bioinspired composites with high impact resistance. As a preliminary study, only FEM simulations were conducted in the current work. To validate the computational results and further the development of the nacre-inspired composites, experimental work needs to be done in the field, and it is also one of the research foci of our following work. As the additive manufacturing (i.e., 3D printing) technology is fast developing and widely used in many fields, there is no technical challenge to fabricate prototypical composites with the ingenious “brick-and-mortar” microstructures. More relevant works are hopefully to be reported in the near future.

CRediT authorship contribution statement

Qiang Zhang: Conceptualization, Investigation, Software, Methodology, Validation, Writing – original draft. **Hao Li:** . **Yuan Liu:** Validation. **Zuoqi Zhang:** Conceptualization, Methodology, Supervision, Funding acquisition, Writing – review & editing. **Yanan Yuan:**

Conceptualization, Methodology, Supervision, Funding acquisition, Writing – review & editing.

Declaration of Competing Interest

The authors declare that they have no known competing financial interests or personal relationships that could have appeared to influence the work reported in this paper.

Acknowledgements

The authors are grateful for the funding support of National Natural Science Foundation of China (Grant Nos. 11720101002, 11772240, 12002244, 11542001, 11502175), Jiangsu Natural Science Foundation (Grant No. BK20150381), Fundamental Research Funds for the Central Universities (2042019kf0223, 2042019kf0039, 2042020kf1035), Translational Medicine and Interdisciplinary Research Joint Fund of Zhongnan Hospital of Wuhan University (Grant No. ZNJC201927) and the Innovative Group Development Program at School of Civil Engineering, Wuhan University.

References

[1] Flores-Johnson EA, Shen L, Guiamatsia I, Nguyen GD. Numerical investigation of the impact behaviour of bioinspired nacre-like aluminium composite plates. Compos Sci Technol 2014;96:13–22.
[2] McKittrick J, Chen PY, Tombolato L, Novitskaya EE, Trim MW, Hirata GA, et al. Energy absorbent natural materials and bioinspired design strategies: A review. Mater Sci Eng, C 2010;30:331–42.
[3] Huang J, Durden H, Chowdhury M. Bio-inspired armor protective material systems for ballistic shock mitigation. Mater Des 2011;32:3702–10.
[4] Essabir H, Hilali E, Elgharad A, El Minor H, Imad A, Elamraoui A, et al. Mechanical and thermal properties of bio-composites based on polypropylene reinforced with Nut-shells of Argan particles. Mater Des 2013;49:442–8.
[5] Liu P, Zhu D, Yao Y, Wang J, Bui TQ. Numerical simulation of ballistic impact behavior of bio-inspired scale-like protection system. Mater Des 2016;99:201–10.
[6] Barthelat F. Biomimetics for next generation materials. Philos Trans A Math Phys Eng Sci 2007;365:2907–19.
[7] Alghamdi S, Du F, Yang J, Pinder G, Tan T. Tensile and shear behavior of microscale growth layers between nacre in red abalone. J Mech Phys Solids 2020;138:103928.
[8] Espinosa HD, Rim JE, Barthelat F, Buehler MJ. Merger of structure and material in nacre and bone – Perspectives on de novo biomimetic materials. Prog Mater Sci 2009;54:1059–100.
[9] Chen P-Y, McKittrick J, Meyers MA. Biological materials: Functional adaptations and bioinspired designs. Prog Mater Sci 2012;57:1492–704.
[10] Mayer G. Rigid biological systems as models for synthetic composites. Science 2005;310:1144–7.
[11] Kakisawa H, Sumitomo T. The toughening mechanism of nacre and structural materials inspired by nacre. Sci Technol Adv Mater 2011;12:14.
[12] Wegst UGK, Ashby MF. The mechanical efficiency of natural materials. Phil Mag 2004;84:2167–86.
[13] Barthelat F, Espinosa HD. An Experimental Investigation of Deformation and Fracture of Nacre-Mother of Pearl. Exp Mech 2007;47:311–24.
[14] Currey JD. Mechanical properties of mother of pearl in tension. Proc Roy Soc Lond Ser B Biol Sci 1997;196:443–63.
[15] Barthelat F, Zhu D. A novel biomimetic material duplicating the structure and mechanics of natural nacre. J Mater Res 2011;26:1203–15.
[16] Børvik T, Hopperstad OS, Pedersen KO. Quasi-brittle fracture during structural impact of AA7075-T651 aluminium plates. Int J Impact Eng 2010;37:537–51.
[17] Humburg H, Zhu D, Beznia S, Barthelat F. Bio-inspired tapered fibers for composites with superior toughness. Compos Sci Technol 2012;72:1012–9.
[18] Sun J, Bhushan B. Hierarchical structure and mechanical properties of nacre: a review. RSC Adv 2012;2:7617.
[19] Yao H, Song Z, Xu Z, Gao H. Cracks fail to intensify stress in nacreous composites. Compos Sci Technol 2013;81:24–9.
[20] Rabiei R, Bekah S, Barthelat F. Failure mode transition in nacre and bone-like materials. Acta Biomater 2010;6:4081–9.
[21] Katti KS, Katti DR, Pradhan SM, Bhosle A. Platelet interlocks are the key to toughness and strength in nacre. J Mater Res 2011;20:1097–100.
[22] Sen D, Buehler MJ. Structural hierarchies define toughness and defect-tolerance despite simple and mechanically inferior brittle building blocks. Sci Rep 2011;1:35.
[23] Dimas LS, Bratzel GH, Eylon I, Buehler MJ. Tough Composites Inspired by Mineralized Natural Materials: Computation, 3D printing, and Testing. Adv Funct Mater 2013;23:4629–38.
[24] Narducci F, Pinho ST. Exploiting nacre-inspired crack deflection mechanisms in CFRP via micro-structural design. Compos Sci Technol 2017;153:178–89.
[25] Dimas LS, Buehler MJ. Modeling and additive manufacturing of bio-inspired composites with tunable fracture mechanical properties. Soft Matter 2014;10:4436–42.
[26] Shao Y, Zhao H-P, Feng X-Q, Gao H. Discontinuous crack-bridging model for fracture toughness analysis of nacre. J Mech Phys Solids 2012;60:1400–19.
[27] Espinosa HD, Juster AL, Latourte FJ, Loh OY, Gregoire D, Zavattieri PD. Tablet-level origin of toughening in abalone shells and translation to synthetic composite materials. Nat Commun 2011;2:173.
[28] Zhang Y, Yao H, Ortiz C, Xu J, Dao M. Bio-inspired interfacial strengthening strategy through geometrically interlocking designs. J Mech Behav Biomed Mater 2012;15:70–7.
[29] Alghamdi S, Tan T, Hale-Sills C, Vilmont F, Xia T, Yang J, et al. Catastrophic failure of nacre under pure shear stresses of torsion. Sci Rep 2017;7:13123.
[30] Alghamdi S, Du F, Yang J, Tan T. The role of water in the initial sliding of nacreous tablets: Findings from the torsional fracture of dry and hydrated nacre. J Mech Behav Biomed Mater 2018;88:322–9.
[31] Alghamdi S, Liu Z, Du F, Yang J, Dahmen KA, Tan T. Sliding Avalanches Between Nacreous Tablets. Nano Lett 2020;20:5024–9.
[32] Wen Xie YY, Zhang Z. A Floquet-Based Bar-Spring Model for the Dynamic Modulus of Bioinspired Composites With Arbitrary Staggered Architectures. J Appl Mech 2019;86:091007.
[33] Geng K, Xie W, Chen B, Yin Q, Yuan Y, Zhang Z. Failure simulation and design optimization of bioinspired heterogeneous interfaces by Floquet-based bar-spring model. Compos Struct 2020;252:112665.
[34] Barthelat F, Tang H, Zavattieri P, Li C, Espinosa H. On the mechanics of mother-of-pearl: A key feature in the material hierarchical structure. J Mech Phys Solids 2007;55:306–37.
[35] Tang H, Barthelat F, Espinosa HD. An elasto-viscoplastic interface model for investigating the constitutive behavior of nacre. J Mech Phys Solids 2007;55:1410–38.
[36] Ren F, Wan X, Ma Z, Su J. Study on microstructure and thermodynamics of nacre in mussel shell. Mater Chem Phys 2009;114:367–70.
[37] Meyers MA, Lin AY, Chen PY, Muyco J. Mechanical strength of abalone nacre: role of the soft organic layer. J Mech Behav Biomed Mater 2008;1:76–85.
[38] Li X, Huang Z. Unveiling the formation mechanism of pseudo-single-crystal aragonite platelets in nacre. Phys Rev Lett 2009;102:075502.
[39] Yi Wen YY, Zhang Z. Study on friction and energy dissipation mechanism of mineral asperities at the interface of nacre. Acta Mech Solida Sin 2021;42:45–52.
[40] Askarinejad S, Rahbar N. Toughening mechanisms in bioinspired multilayered materials. J R Soc Interface 2015;12:20140855.
[41] Djumas L, Molotnikov A, Simon GP, Estrin Y. Enhanced Mechanical Performance of Bio-Inspired Hybrid Structures Utilising Topological Interlocking Geometry. Sci Rep 2016;6:26706.
[42] Askarinejad S, Choshali HA, Flavin C, Rahbar N. Effects of tablet waviness on the mechanical response of architected multilayered materials: Modeling and experiment. Compos Struct 2018;195:118–25.
[43] Narducci F, Lee KY, Pinho ST. Realising damage-tolerant nacre-inspired CFRP. J Mech Phys Solids 2018;116:391–402.
[44] Tran P, Ngo TD, Mendis P. Bio-inspired composite structures subjected to underwater impulsive loading. Comput Mater Sci 2014;82:134–9.
[45] Tang Z, Kotov NA, Magonov S, Ozturk B. Nanostructured artificial nacre. Nat Mater 2003;2:413–8.
[46] Munch E, Launey ME, Alsem DH, Saiz E, Tomsia AP, Ritchie RO. Tough, Bio-Inspired Hybrid Materials. Science. 2008;322:1516–20.
[47] Yin Z, Hannard F, Barthelat F. Impact-resistant nacre-like transparent materials. Science. 2019;364:1260–3.
[48] Shi Y, Swait T, Soutis C. Modelling damage evolution in composite laminates subjected to low velocity impact. Compos Struct 2012;94:2902–13.
[49] Pedro P. Camanho, Dávila CG. Mixed-mode decohesion finite elements for the simulation of delamination in composite materials. Tech Rep NASA/TM-2002-211737. 2002.